

ARTICLE



Characterization and identification of measurable endpoints in a mouse model featuring age-related retinal pathologies: a platform to test therapies

Mayur Choudhary¹, Faryan Tayyari¹, James T. Handa² and Goldis Malek^{1,3}✉

© The Author(s), under exclusive licence to United States and Canadian Academy of Pathology 2022

Apolipoprotein B100 (apoB100) is the structural protein of cholesterol carriers including low-density lipoproteins. It is a constituent of sub-retinal pigment epithelial (sub-RPE) deposits and pro-atherogenic plaques, hallmarks of early dry age-related macular degeneration (AMD), an ocular neurodegenerative blinding disease, and cardiovascular disease, respectively. Herein, we characterized the retinal pathology of transgenic mice expressing mouse *apoB100* in order to catalog their functional and morphological ocular phenotypes as a function of age and establish measurable endpoints for their use as a mouse model to test potential therapies. *ApoB100* mice were found to exhibit an age-related decline in retinal function, as measured by electroretinogram (ERG) recordings of their scotopic a-wave, scotopic b-wave; and c-wave amplitudes. *ApoB100* mice also displayed a buildup of the cholesterol carrier, apolipoprotein E (apoE) within and below the supporting extracellular matrix, Bruch's membrane (BrM), along with BrM thickening, and accumulation of thin diffuse electron-dense sub-RPE deposits, the severity of which increased with age. Moreover, the combination of *apoB100* and advanced age were found to be associated with RPE morphological changes and the presence of sub-retinal immune cells as visualized in RPE-choroid flatmounts. Finally, aged *apoB100* mice showed higher levels of circulating and ocular pro-inflammatory cytokines, supporting a link between age and increased local and systemic inflammation. Collectively, the data support the use of aged *apoB100* mice as a platform to evaluate potential therapies for retinal degeneration, specifically drugs intended to target removal of lipids from Bruch's membrane and/or alleviate ocular inflammation.

Laboratory Investigation (2022) 102:1132–1142; <https://doi.org/10.1038/s41374-022-00795-7>

INTRODUCTION

Age-related macular degeneration (AMD) is the leading cause of vision loss among the elderly in the western world¹. Approximately 80% of patients with AMD are diagnosed with the early dry subtype, characterized by the accumulation of lipid and protein filled material within and extracellular to the retinal pigment epithelium (RPE)^{2–4}. To date a sundry of genetic and environmental risk factors impacting AMD development and progression have been discovered^{5–7}, precipitating identification of putative pathogenic pathways important in promoting salient disease features. However, because central etiologic aspects of early dry AMD remain elusive, no therapeutic options have been developed for this subset of patients. This unmet need is the driving factor for not only further characterizing the pathobiology of AMD and discovering novel disease mechanisms, but also delineating retinal function and morphology of potential animal models that may be used as a pre-clinical platform to test potential therapies.

To date, the most common strategies used for creating pre-clinical animal models of AMD have relied on targeted modulations of genetic and environmental risk factors, in particular, in mice^{8,9}. Another strategy commonly used with *in vivo* modeling has been the modulation of pathogenic pathways associated with

AMD onset and progression, including the administration of chemical oxidizing agents to induce injury such as sodium iodate^{10–13}. Arguably, two consistently reported potential AMD-related pathogenic pathways have been dysregulation of lipid homeostatic and immune pathways^{8,14–17}. Specifically, neutral lipids continuously accumulate in the multi-laminar extracellular matrix called Bruch's membrane (BrM) of normal eyes with aging¹⁸. This buildup of extracellular lipid rich deposits and inflammatory material, within and below the RPE in the form of basal laminar deposits, basal linear deposits, and drusen, are key histopathologic and clinical findings that separate aging-related changes from early, dry AMD².

Studies on the composition of these lipid deposits and their potential sources have been carried out in some detail^{18–23}, and resulted in identification of cholesterol carriers such as apolipoprotein B (apoB)^{18,21,24–26}. Apolipoproteins, are amphipathic molecules involved in lipid delivery, acceptance and modification, which along with phospholipids, triglycerides and cholesterol esters, are constituents of lipoprotein complexes²⁷. ApoB protein localizes to Bruch's membrane and drusen^{21,28,29}, and its gene presents as either full length (*apoB100*) or a truncated variant (*apoB48*). While, apoB100 is a component of several atherogenic

¹Department of Ophthalmology, Duke University School of Medicine, Durham, NC, USA. ²Wilmer Eye Institute, Johns Hopkins School of Medicine, Baltimore, MD, USA.

³Department of Pathology, Duke University School of Medicine, Durham, NC, USA. ✉email: gmalek@duke.edu

Received: 21 February 2022 Revised: 13 April 2022 Accepted: 18 April 2022

Published online: 19 May 2022

lipoproteins including low-density lipoproteins (LDL), very LDL (VLDL), and intermediate LDL (IDL), apoB48 (apoB48), is the major protein component of chylomicrons²⁷. Importantly, the accumulation of apoB has been indicated as an initiator and sustainer of inflammation, another important factor in AMD development and progression.

Mice have a similar RPE and rod/cone photoreceptor density to the human perifovea, the location of the earliest AMD changes³⁰. Thus, mice are a reasonable model to study early AMD pathogenesis. However, due to the strong effects of the editing enzyme APOBEC1, mice predominantly produce apoB48 and minimal apoB100. With this in mind and given that apoB accumulates within human Bruch's membrane and drusen^{21,28,29}, the ocular morphology of a transgenic mouse model, which exclusively expresses *apoB100*³¹, was investigated by Fujihara et al.³². They found that the RPE-choroid in these mice produce apoB100, as detected by metabolic labeling, gene expression, and immunohistochemical staining³². Additionally, they found that cholesterol ester deposition within BrM of *apoB100* mice did not vary in young mice aged between 2 and 8 months. Since advanced age drives AMD development, in the current study, we set out to comprehensively characterize ocular morphology and retinal function, in vivo, and morphological changes, ex vivo, evaluating histology at the ultrastructural level in middle aged (8–12-month-old) and old (17–21-month-old and 24–28-month-old) *apoB100* mice, the latter of which is comparable in age to the risk age for AMD in humans. We found that in *apoB100* mice, retinal function, as evaluated with electroretinography (ERG), declines with age effecting photopic b-wave, scotopic a-, b-wave, and c-wave amplitudes. Clinically, *apoB100* mice, as observed by fundus imaging and optical coherence tomography (OCT), develop scattered lesions in the inner and outer retina which increase in frequency with age. Histopathologically, neutral lipids and apolipoprotein E (apoE) accumulate in BrM and in thin diffuse sub-retinal pigment epithelial (sub-RPE) lesions, concomitant with the accumulation of sub-retinal immune cells at the RPE layer, and in regions of RPE atrophy. Overall, with age, *apoB100* mice develop morphological and molecular features similar to that observed in early AMD that can be evaluated experimentally. Furthermore, our comprehensive characterization of this mouse model supports its use as a platform to test potential therapeutics targeting ocular degenerative diseases associated with aging, such as AMD, that present with retinal degeneration and ocular inflammation.

MATERIALS AND METHODS

Transgenic mouse model

Male and female *apoB100* on a *C57/S129* background or *C57/S129* mice *B6.129³²* (from the Handa Lab and available from Jackson Laboratories, Bar Harbor, ME, USA) were maintained in a temperature (25 °C) and light controlled (12 h light/12 h dark) environment, provided standard mouse chow and water ad libitum. The *apoB100* mice (Strain #:002877; *B6;129S7-ApoB^{tm2Sgy/J}*) were generated after a CTA to TTA mutation was introduced to sequences corresponding to the *apoB48* editing codon (codon 2179) in exon 26. While the expression of *apoB100* is unaffected by this mutation, little to no *apoB48* is produced. As mentioned in the original publication by Farese et al.³¹ the genetic background of the mice was described as 50% *C57BL/6* and 50% *129/Sv³¹*. All mice were screened for the retinal degeneration 8 (*rd8*) mutation as previously described (Fig. S1)³³. Briefly, DNA was isolated from mouse tail biopsy samples (<5 mm) by incubating them for 24 h at 55 °C in lysis buffer (10 mM Tris, 100 mM NaCl, 10 mM EDTA, 0.5% SDS, 4 mg/ml Proteinase K). The mutation was identified using a method described by Mehalow et al.³⁴. Primer sequences are as follows: mCrb1 mF1: GTGAAGACAGCTACAGTTCTGATC; mCrb1 mF2: GCCCTGTITG CATGGAGAACTTGGAAAGACAGCTACAGTTCTCTG; and mCrb1 mR: GCCC CATTGGCACTGATGAC. For PCR amplification at least 25 ng DNA was used in a 14 µl reaction volume containing ReadyMix™ REDTaq[®] PCR reaction mix (Sigma-Aldrich, St Louis, MO) along with 10 µM each of forward and reverse primers for wild-type allele. A similar reaction mixture was prepared with forward and reverse primers for the *rd8* mutant allele.

Reactions initially were denatured at 94 °C for 5 min followed by 35 cycles at 94 °C for 30 s, 65 °C for 30 s, 72 °C for 30 s and a final extension at 72 °C for 7 min. Amplicons were separated on a 3% agarose gel and visualized under UV light after staining with ethidium bromide. Mice were weighed and blood samples were collected at the time of euthanasia. Enucleated eyes were collected, preserved for light and electron microscopy as previously described³⁵.

In vivo imaging

Fundus images were obtained using a Micron IV (Phoenix Research Laboratories Inc, Pleasanton, CA) retinal imaging microscope from anesthetized *apoB100* mice (8–12-month old: *n* = 13; 17–21-month old: *n* = 4; 24–28-month old: *n* = 2). The OCT module of the Micron IV was used to image retinal layers guided from the bright field.

Electroretinography (ERG)

ERGs were recorded using the Espion E² system (Diagnosys LLC) as described previously³³. Briefly, 8–12-month-old (*n* = 5) and 17–21-month-old (*n* = 5) *apoB100* mice were dark-adapted for 4 h and anesthetized by an intra-peritoneal injection of a ketamine/xylazine mixture (85/10 mg/kg). Pupils were dilated with 1% cyclopentolate-HCl and 2.5% phenylephrine, and the mouse body temperature was maintained at 37 °C using a water-based warming pad. ERG responses under dark-adapted (scotopic) conditions were evoked by a series of nine flashes ranging from 0.0001 cd·s/m² to 100 cd·s/m². For flashes up to 0.1 cd·s/m², responses of 10 trials were averaged. For 0.5 and 1 cd·s/m² flash responses, three trials were averaged. For brighter stimuli, responses to single flashes were recorded without averaging. Light-adapted (photopic) ERGs were evoked by a series of six flashes ranging from 0.2 cd·s/m² to 2000 cd·s/m² where rod inputs were suppressed with a steady background illumination of 50 cd/m². Up to 10 trials were averaged for all flash responses. Analysis of a- and b-wave amplitudes was performed as previously described³³. For c-waves, flash responses (5 cd·s/m² to 100 cd·s/m²) were recorded for 7 s (8–12-month old, *n* = 12; 17–21-month old, *n* = 5).

Optokinetic response

Visual acuity was measured using an Optometry System (CerebralMechanics Inc., Lethbridge, Alberta, Canada), as previously described³⁶. After disinfecting the platform to remove a prior mouse's scent, mice were placed on the platform for 5 min to habituate. An observer assessed for reflexive head-tracking movements that correlated with the frequency of the virtual sine wave grating on the monitors using 100% contrast in normal lighting conditions. The visual acuity threshold was determined at the highest spatial frequency (cycle/degree) when the animal stopped tracking. Right and left eyes were tested separately and averaged together to get one spatial frequency per animal. Analyses was performed in young (3-month old, *n* = 4–5 mice per genotype) and old (17-month old) mice (*n* = 5 mice per genotype).

Transmission electron microscopy (TEM)

For visualization of ocular morphology with electron microscopy, eyes were fixed in 2% glutaraldehyde, post fixed in 1% osmium tetroxide, and embedded in Spurr's resin^{33,35}. Morphology of the retina/RPE/choroid was examined in 1 µm toluidine blue stained plastic sections. An image of the whole retinal cross-section was created by stitching overlapping images in Adobe Photoshop CS4. Ultrastructural details of the retina/RPE/choroid complex were visualized in thin sections (15–20 images per eye, 8–12-month old, *n* = 4 eyes; 17–21-month old, *n* = 3 eyes). BrM thickness was measured at ten random locations along the length of the section and averaged to calculate mean BrM thickness (8–12-month old, *n* = 4 eyes; 17–21-month old, *n* = 3 eyes). Percentage of BrM length exhibiting sub-RPE deposits was quantified. Briefly, the length of BrM exhibiting sub-RPE deposits was measured randomly in ten images (every 4th image along the length of section) per eye (*n* = 3 eyes per group) and divided by the total length of BrM in that image. The results from each eye were averaged and plotted as percentage of BrM length with sub-RPE deposits.

Immunohistochemistry and morphology

For immunohistochemistry, cryosections from the nasal, central, and peripheral regions of the eye were probed with antibodies listed in Supplementary Table 1. Non-specific immunostaining in sections was blocked with normal serum (Jackson Immunoresearch, West Grove, PA,

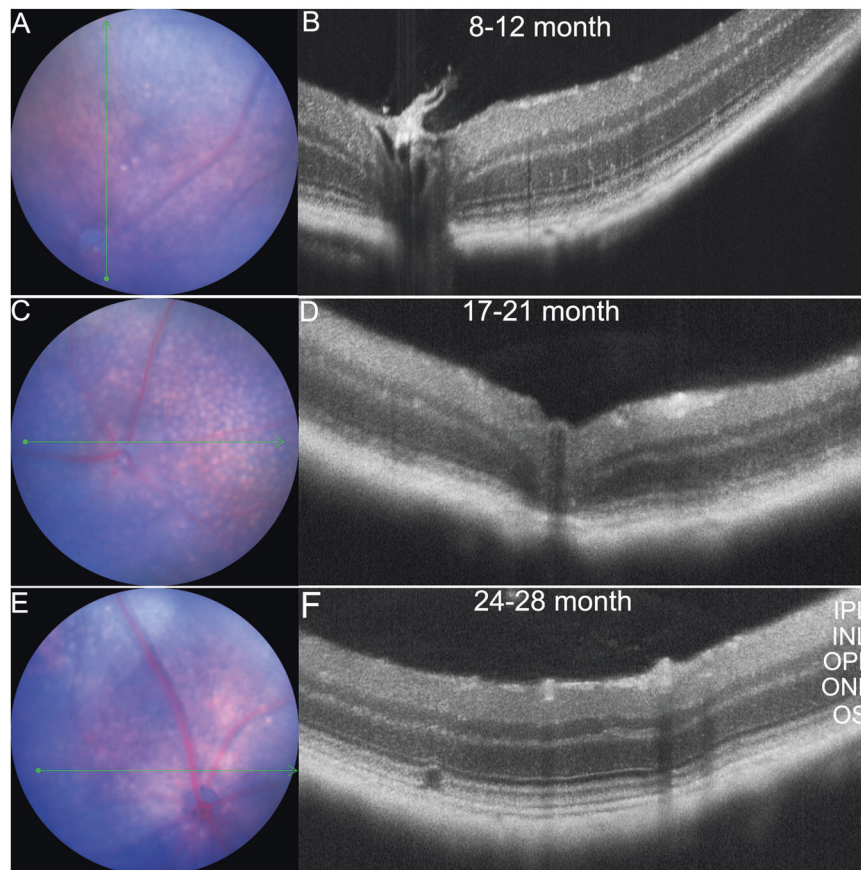


Fig. 1 In vivo imaging of *apoB100* mouse eyes. A Micron IV retinal imaging microscope was used to acquire fundus and OCT images. Representative images of *apoB100* (A, B) 9-month-old, male, left eye (oculus sinister OS), C, D 21-month-old, female, OS, and E, F 28-month-old, female, OS. OCT slice corresponds to the green arrow in the fundus images (INL Inner nuclear layer, IPL Inner plexiform layer, ONL Outer nuclear layer, OPL Outer plexiform layer, OS Photoreceptor outer segments).

USA) appropriate to the secondary antibody species. Secondary antibodies were conjugated to AlexaFluor 568 or 488 (Invitrogen). Control slides containing sequential sections were probed with non-immune serum and buffer without primary antibody. Nuclei were stained with Hoechst 33258 (Invitrogen). Images were collected on a C2si confocal microscope (Nikon Corporation, Tokyo, Japan) and visualized using Adobe Photoshop CS4. Fluorescent intensity from anti-apolipoprotein E probed sections was quantified using ImageJ software. Briefly, the RGB images were converted to gray scale and regions of apolipoprotein E immunoreactivity were selected along the length of the BrM, followed by measuring mean intensity. RPE/choroid flatmounts were prepared from enucleated eyes as described³⁷, and stained with phalloidin-tetramethylrhodamine B isothiocyanate³⁵ and probed with an antibody to F4/80 to visualize RPE cell borders and immune cells, respectively. Nuclei were stained with Hoechst 33258³⁵ (Invitrogen). Images were collected on a Nikon C2si confocal microscope, visualized and processed using Nikon Elements software to display maximum intensity projection. Images from each quadrant of the stained RPE-choroid flatmounts were stitched using Adobe Photoshop CC to obtain an image of the complete RPE-choroid flatmount and F4/80⁺ cells were counted per flatmount (8–12-month old, $n = 5$; 17–21-month old, $n = 5$; 24–28-month old, $n = 2$).

Cytokine analysis

Plasma was collected, and the RPE/choroid complex was isolated from posterior eyecups of *apoB100* mice (8–12-month old, $n = 4$; 17–21-month old, $n = 4$) and homogenized in RIPA buffer, as previously described^{35,38}. Protein was quantified using the BCA assay, used to normalize protein amounts loaded onto each Mouse Cytokine Array C3 membrane (RayBiotech, Norcross, GA). Each group had two technical and four biological replicates. The manufacturer's protocol was followed for processing the membranes. Images of the membranes were inverted to neutralize the effect of any differences in background, and dot intensity

was quantified using ImageJ. Since each antibody on the membrane was blotted in duplicate, the mean intensity of the dots was calculated, averaged across the biological replicates and normalized to the positive control on the blot.

Statistical methods and rigor

Statistical methods for data analysis included two-tailed Student's t test and multiple t tests with Holm-Sidak correction for multiple comparisons (as recommended by GraphPad Prism) using GraphPad Prism. Values were considered statistically significant at $p < 0.05$ and are indicated in the figures.

RESULTS

Ocular pathologies of *apoB100* mice worsen with age

To characterize the effect of background strain on retinal morphology, eyes of 8–12-month-old *C57BL/6J* (Fig. S2a, b), *B6.129* (Fig. S2c, d), and *apoB100* (Fig. S3a–h) mice were imaged by a Micron IV retinal microscope and fundus and OCT images were acquired. While no clear phenotypic differences were observed between *C57BL/6J* and *B6.129* mice, at 8–12 months of age, several pathologic features were observed in *apoB100* mice as detailed below. The effect of age on retinal morphology in *apoB100* mice was imaged in eyes of 8–12-month (Fig. 1A, B), 17–21-month (Fig. 1C, D), and 24–28-month-old mice (Fig. 1E, F). A spectrum of lesions was seen on OCT images that included inner retinal hyper-reflective spots, sub-retinal edema, and localized deposits (Figs. 1, S3, S4). The number and size of the lesions varied between eyes and the phenotype worsened with age (Supplementary Table 2 and Figs. S3, S4). Briefly, hyper-reflective spots in the inner retina were

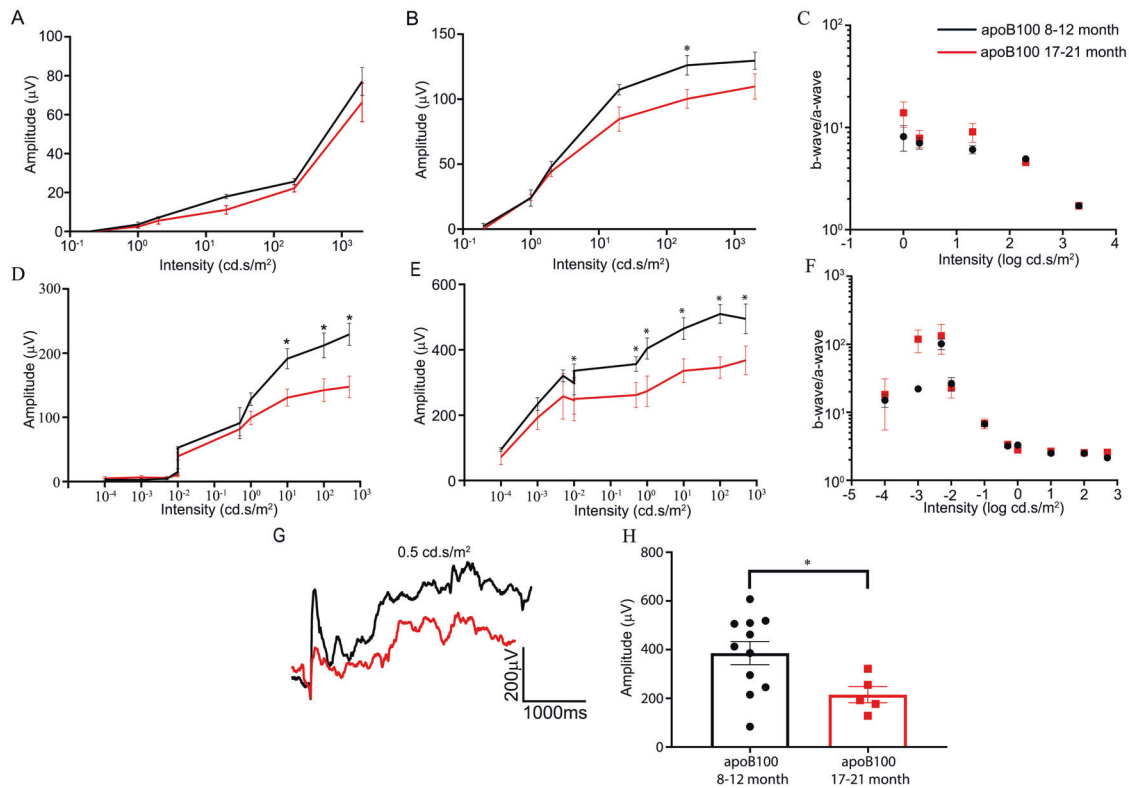


Fig. 2 Retinal function of *apoB100* mice with age. Averaged ERG responses in 8–10-month-old (black) and 17–21-month-old (red) dark-adapted *apoB100* mice (red) ($n = 5$ per group). Plots of **A** photopic a-wave amplitudes, **B** photopic b-wave amplitudes, **C** photopic b-wave/a-wave ratio, **D** scotopic a-wave amplitudes, and **E** scotopic b-wave amplitudes and **F** scotopic b-wave/a-wave ratio are shown as a function of flash intensity (for some points, the error bars are shorter than the height of the symbol). Data points are mean and SEM. $*p < 0.01$. **G** Representative ERG traces from 8–10-month-old (black) and 17–21-month-old (red) dark-adapted *apoB100* mice. **H** Averaged c-wave amplitudes in 8–10-month-old ($n = 11$) and 17–21-month-old ($n = 5$) *apoB100* mice at a flash intensity of 0.2 cd.s/m². Data points are mean \pm SEM (8–12 month, $n = 11$, 17–21 month, $n = 5$, $*p < 0.05$).

observed in 60.9% eyes from mice aged 8–12 month, 77.8% aged 17–21-month, and 100% aged 24–28 month. Sub-retinal edema was observed in 26.1% eyes from mice aged 8–12 month, whereas localized deposits were observed in 52.2% eyes from mice aged 8–12 month, 33.3% aged 17–21-month and 50% aged 24–28 month (Supplementary Table 2). Noteworthy, we did not observe retinal folds or pseudorosettes in OCT cross-sections, typically associated with the retinal degeneration 8 (RD8) mutation³⁹. These results demonstrate that mice expressing predominantly *apoB100* develop ocular pathological lesions, similar to those observed in several retinal degenerative diseases and that their phenotype worsens with age.

Retinal function of *apoB100* mice declines with age

To further characterize the ocular function, electroretinography was performed in 8–12-month-old *B6.129* and *apoB100* mice (Fig. S5). *ApoB100* mice exhibited a significant decline in retinal function, specifically in their photopic and scotopic b-wave amplitudes (Fig. S5b, e), as compared to age-matched *B6.129* mice, suggesting potential impairment of post-synaptic neurons. Additionally, a significant decline in c-wave amplitudes (Fig. S5g, h), which reflects RPE function was seen. Measurement of the optokinetic response (OKR) of *B6.129* and *apoB100* mice at 3-month and 17-month of age also revealed a significant genotype-dependent decline in *apoB100* mice (Fig. S6). Importantly, a significant age-dependent reduction in OKR was also observed in *apoB100* mice (Fig. S6). Since, OKR is driven by ON direction-selective retinal ganglion cells, the data suggests a potential impairment at the level of retinal ganglion cells in *apoB100* mice^{40–42}. To further characterize the aging effect in *apoB100* mice, we performed electroretinography in 8–12-month

and 17–21-month-old mice ($n = 5$). Dark-adapted 17–21-month-old mice under scotopic and rod-saturated photopic conditions had smaller averaged b-wave amplitudes compared with 8–12-month-old *apoB100* mice, under both light conditions (Fig. 2B, E). Specifically, 17–21-month-old *apoB100* mice had an $\sim 40\%$ drop in scotopic b-wave (Fig. 2E), 30% decline in photopic b-wave (Fig. 2B), and 40% reduction of a-wave amplitudes in scotopic conditions (Fig. 2D), when the average wave amplitudes were plotted as a function of flash intensity. Since the a-wave amplitude reflects photoreceptor activity and b-wave is a measure of the activity of post-synaptic neurons, we may extrapolate that *apoB100* mice display functional impairment with aging mainly attributable to ON-bipolar cells, and rod photoreceptors. To assess the relative function of the inner retina as compared to the outer retina, we calculated the b-wave/a-wave ratio at each flash intensity and found no significant difference between 8–12-month and 17–21-month-old *apoB100* mice (Fig. 2C, F), suggesting potentially impaired photoreceptors and inner retina. Likewise, the middle and old age groups had similar inner and outer nuclear layers (Figs. S7, S8) and the distribution of the photoreceptor proteins, rhodopsin and R/G opsin had similar immunolocalization patterns and number of nuclei in the outer nuclear layer (Fig. S9a, b). Finally, when retinal cryosections were probed with antibodies to bipolar cell (Protein kinase C- α /PKC α), Müller cell and RPE (Cellular retinaldehyde-binding protein/CRALBP) proteins, we did not observe any remarkable differences between the two cohorts (Fig. S9c, d). Interestingly, c-wave amplitudes, a measure of RPE response, were significantly reduced in 17–21-month-old mice as compared to 8–12-month-old mice (Fig. 2G, H), suggesting an age-related decline in RPE function and potential cell damage. These results indicate

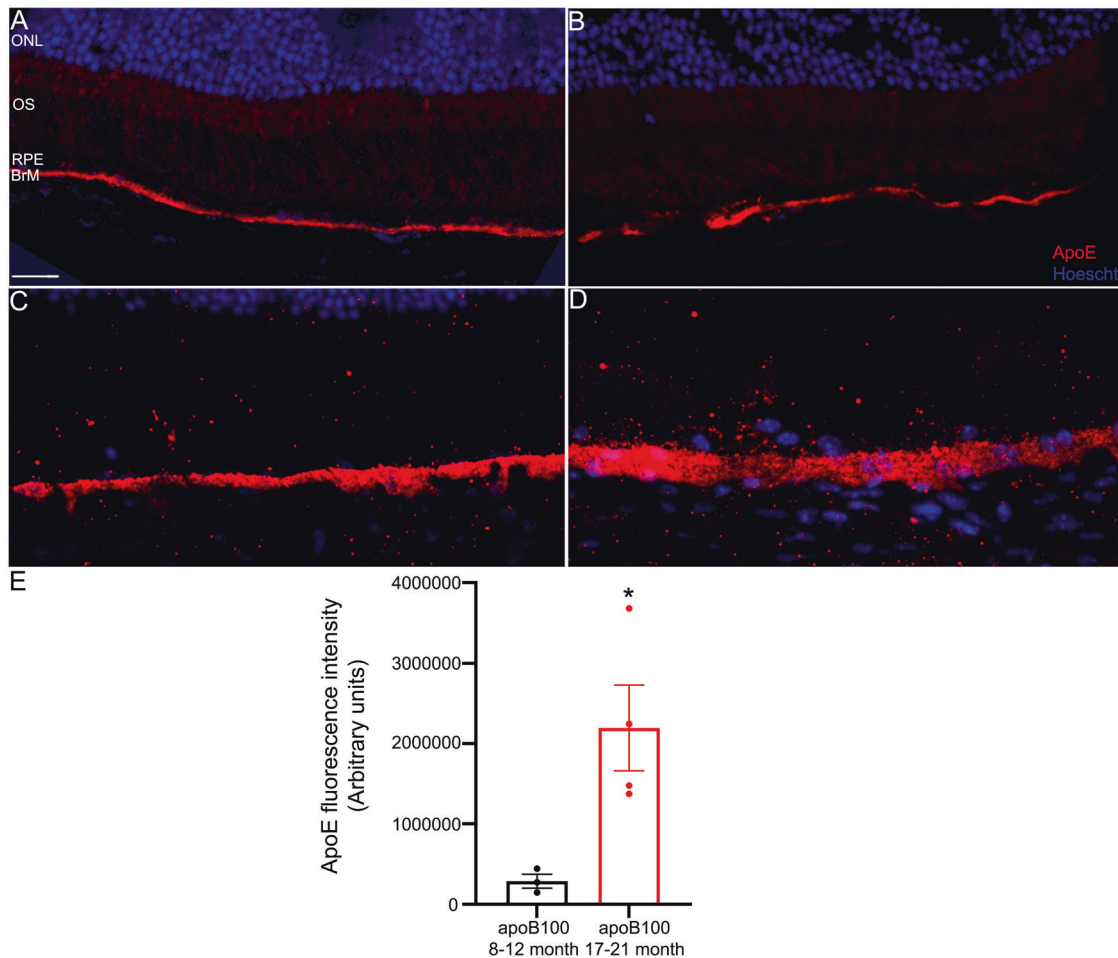


Fig. 3 ApoE accumulates below the RPE and within BrM of aged *apoB100* mice. ApoE stained images of the outer retina of **A, B** 8–12-month-old *apoB100* mice, and **C, D** 17–21-month-old *apoB100* mice, displaying ApoE positive sub-RPE deposits and Bruch’s membrane thickening (Scale bar: 20 μ m). **E** Quantification of ApoE staining intensity in 8–12-month and 17–21-month-old *apoB100* mice (8–12 month, $n = 3$, 17–21 month, $n = 4$, $*p < 0.05$).

that the abnormal pathological features observed via fundus imaging correlate with retinal function impairment in the *apoB100* mice, which worsens with age.

Aged *apoB100* mice accumulate apoE-rich deposits in Bruch’s membrane

Lipid accumulation in Bruch’s membrane extracellular to the RPE is a contributing factor to drusen formation^{24,43}. A defining feature of sub-RPE deposits in AMD is the accumulation of apoE, which regulates the transport of cholesterol and oxidized lipoproteins^{23,44}. An increase in apoE immunoreactivity in RPE cells (Fig. S10b), as well as along the length of BrM in 8–12-month-old *apoB100* mice (Fig. S10c, d) as compared to age-matched *B6.129* mice was observed. We also found a significant increase in apoE immunopositive staining along the length of BrM in 17–21-month-old mice (Fig. 3C–E) as compared to 8–12-month-old mice (Fig. 3A, B, E), supporting potential accumulation of apoE containing lipoproteins along BrM as a function of age and pathology^{21,22}.

ApoB100 mice develop an AMD-like ultrastructural pathology that worsens with age

High magnification evaluation of the outer retina of *apoB100* mice using TEM allowed us to visualize the ultrastructure of the RPE-choroid. Whereas, 8–12-month-old mice exhibited areas of normal RPE-choroid morphology showing organized basal infoldings and apical processes of the RPE interspersed between regions with

disrupted basal infoldings and sub-RPE basal deposits (Fig. 4A, B), the 17–21-month-old mice displayed relatively smaller regions of normal RPE pathology and a higher degree and prevalence of loss of or disrupted basal infoldings, thin diffuse sub-RPE deposits containing electron-dense material, and BrM thickening (Fig. 4C, D). 8–12-month-old *apoB100* mice also develop lipid droplets within BrM (Fig. 4E–H). The older mice displayed a more severe phenotype with lipid droplets in the RPE, greater disruption of the basal infoldings, and thicker and more electron-dense sub-RPE basal deposits than younger mice (Fig. 4I, J). Additionally, BrM appeared as continuous regions of electron-dense material as compared to the 8–12-month-old mice (Fig. 5K, L). BrM was thicker, the percentage of BrM length exhibiting sub-RPE deposits, and the prevalence of sub-RPE deposits was significantly increased in the older cohort as compared to 8–12-month-old *apoB100* mice (Fig. S11a, b). RPE apical processes and photoreceptor outer segments displayed normal morphology in both the cohorts. These characteristics strongly suggest an association between *apoB100* and accumulation of lipids and development of RPE degenerative AMD-like features in the outer retina that develop with age.

RPE cell damage is coupled with buildup of immune cells in the sub-retinal space

We next examined RPE morphology by preparing RPE-choroid flatmounts, followed by staining with phalloidin to delineate RPE

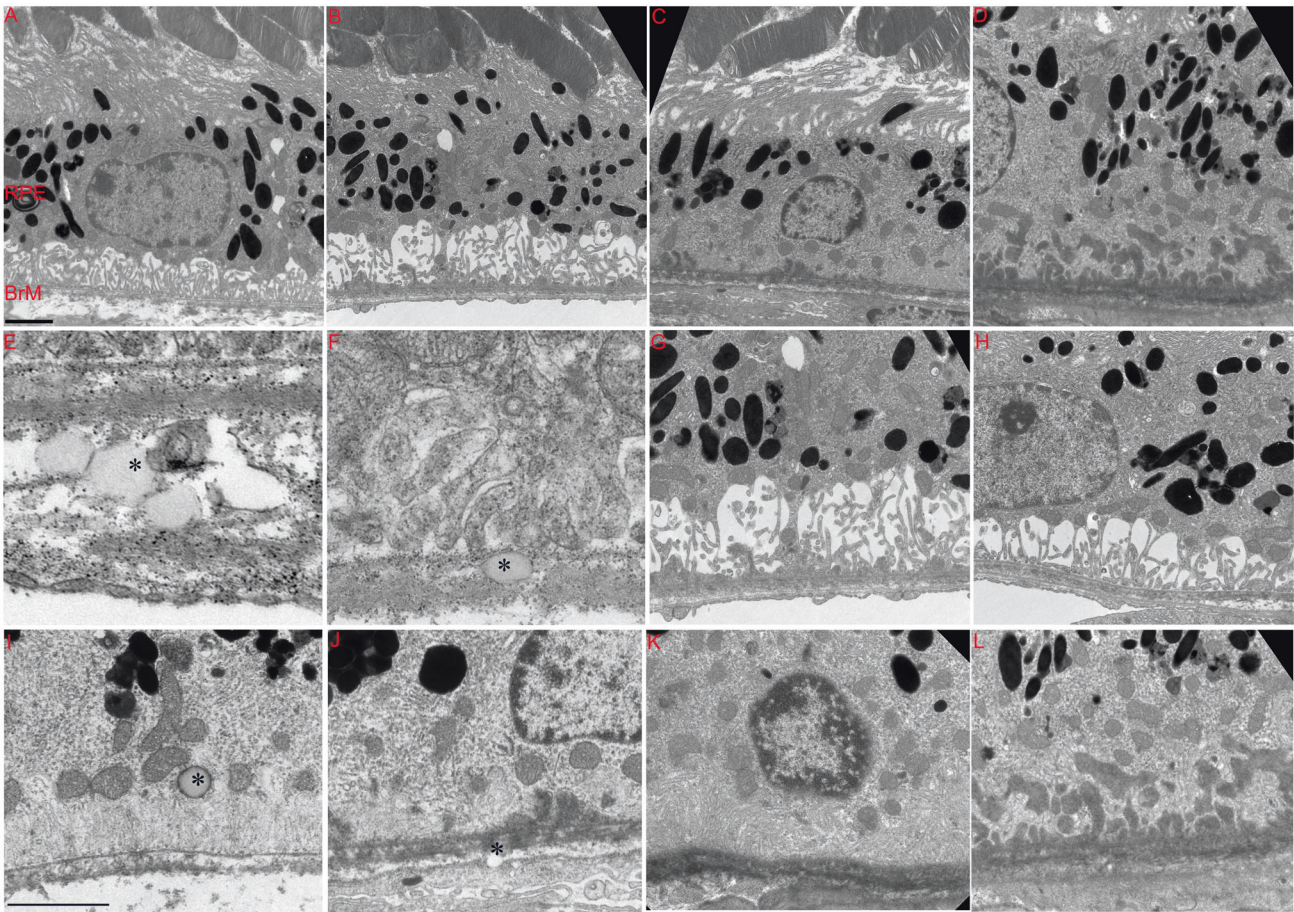


Fig. 4 Ultrastructural changes in *apoB100* as a function of age. **A, B** Low magnification TEM images from 8–12-month-old *apoB100* mice display regions with thin diffuse sub-RPE deposits and disrupted basal infoldings. **C, D** 17–21-month-old mice exhibit continuous thin sub-RPE deposits and a higher degree of disrupted/absent basal infoldings (Scale bar = 2 μ m). **E–H** High magnification images of 8–12-month-old mice exhibit lipid droplets (asterisks) in BrM. **I–L** 17–21-month-old mice display BrM thickening and sub-RPE deposits in addition to lipid droplets in the RPE as well as BrM (asterisk; Scale bar = 2 μ m).

cell shape and probing with a macrophage antibody, F4/80, to visualize the presence of immune cells. Sub-retinal F4/80-positive were noted in the posterior pole and were increased 2-fold in the number in the 17–21-month-old cohort (114.2 ± 14.27 , $n = 5$) as compared to 8–12-month old (59.6 ± 18.52 , $n = 5$; Fig. 5A, B, D). Despite the small cohort size for 24–28-month-old *apoB100* mice due to advanced age, this group showed trends towards a decline in the number of sub-retinal immune cells (62.5 ± 8.5 , $n = 2$; not significant), as compared to the 17–21-month-old cohort (Fig. 5C, D). The RPE cell morphology was atrophic and dedifferentiated in the aged mice (Fig. 5E–G). The RPE of 8–12-month-old mice was dysmorphic and enlarged, with sub-retinal immune cells (Fig. 5E), whereas, 17–21-month-old mice had F4/80-positive cells incorporated into the RPE cell layer and appeared to replace some RPE (Fig. 5F). The 24–28-month-old group had regions with extensive damage in the RPE cell layer, characterized by areas of RPE loss and infiltration of immune cells (Fig. 5G). Immunolocalization of macrophages in retina-RPE-choroid cross-sections confirmed the presence of immune cells in the sub-retinal space of 8–12-month-old (Fig. 5H, I) and 17–21-month old (Fig. 5J, K), consistent with the observations seen in the RPE-choroid flatmounts. Interestingly, even in the cross-sections, one F4/80-positive cell can be seen embedded in the same plain as the RPE cell layer (Fig. 5J, asterisk), substantiating the observation seen in the RPE-choroid flatmounts. The F4/80-positive immune cells had different morphologies, ranging from resting (stellate) to activated (ameboid) cells (Fig. 5I2). With activated cells, we next performed cytokine

analysis at the local (RPE-choroid) and systemic (blood plasma) level. Out of a panel of 62 proteins, in blood plasma from 8–12-month-old and 17–21-month-old *apoB100* mice, the levels of three cytokines increased and one decreased (Fig. 6A, B). Specifically, expression of CXC chemokine platelet factor-4 (CXCL-4), macrophage inflammatory protein-2 (MIP-2) and lipopolysaccharide-induced CXC chemokine (LIX) increased significantly, while insulin-like growth factor binding protein-3 (IGFBP-3) expression decreased. On the other hand, RPE-choroid protein samples from 8–12 and 17–21-month-old mice had only two significantly increased cytokines, Interleukin 1-alpha (IL-1 α , also known as IL-1F1) and macrophage inflammatory protein 1-gamma (MIP-1 γ also known as chemokine ligand 9, CCL9; Fig. 6C, D). Finally, we probed retinal cryosections with Glial fibrillary acidic protein (GFAP) to evaluate potential changes in reactive astrocytes. Though GFAP immunoreactivity was evident in the 8–12-month and 17–21-month-old cohorts, its distribution was variable and no significant age-related increase in staining was noted (Fig. S13a, b).

DISCUSSION

Given the principal role aging plays in the development of ocular neurodegenerative diseases such as AMD, it is important to investigate the potential contribution of age to disease development. Herein, we describe the ocular phenotype of *apoB100* mice as a function of age. Our imaging and retinal function studies show that *apoB100* mice develop lesions discernible via fundus

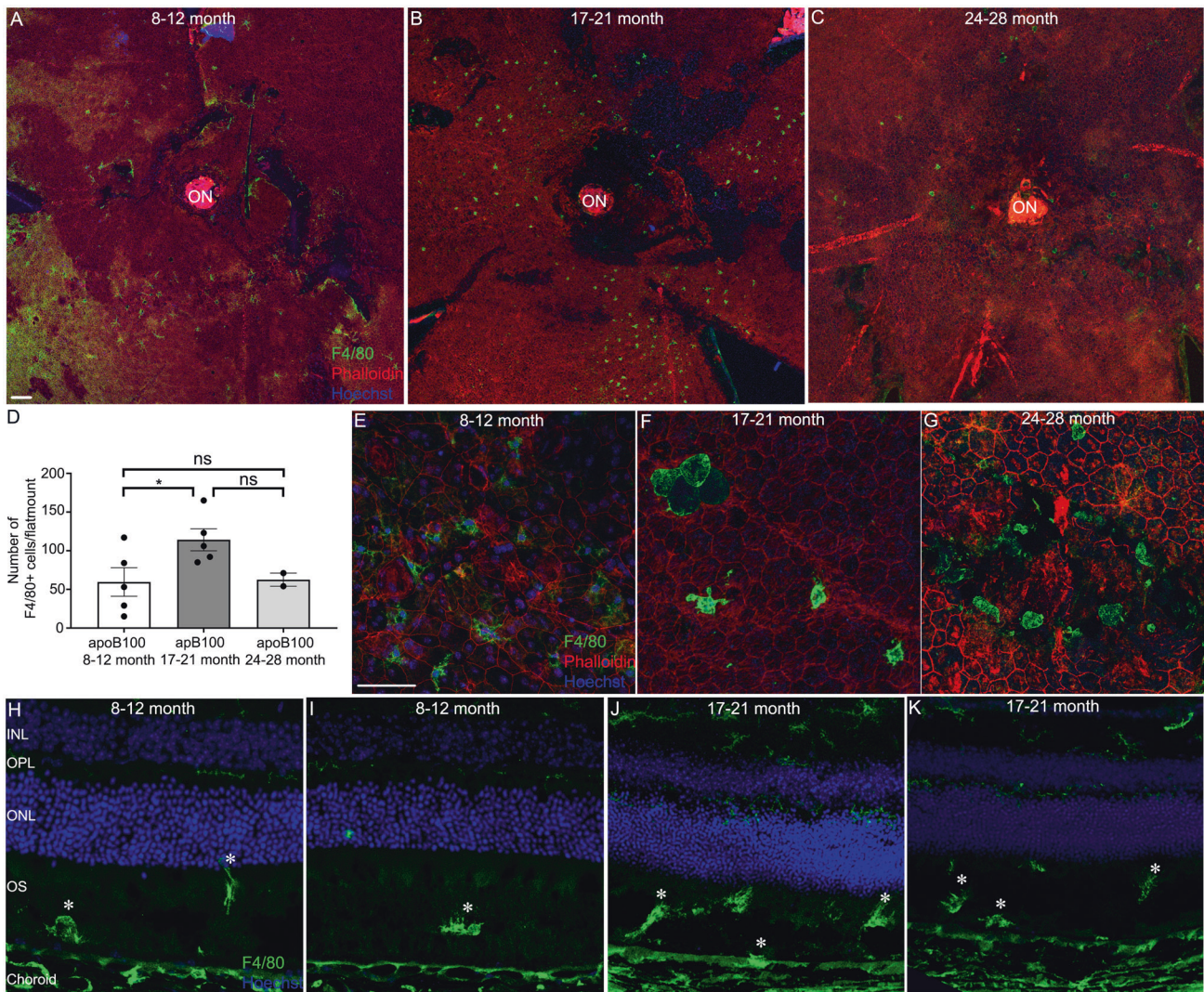


Fig. 5 Distribution of sub-retinal immune cells and RPE degenerative changes in *apoB100* mice increases in severity with age. F4/80 immunoreactivity and Phalloidin stained images of RPE flatmounts from **A** 8–12-month-old (Scale bar: 100 μ m), **B** 17–21-month old, and, **C** 24–28-month-old mice showing the distribution of immune cells in the outer retina and RPE morphology (ON Optic nerve). **D** Quantification of F4/80-positive cells in *apoB100* mice (8–12-month old, $n = 5$, 17–21-month old, $n = 5$, and 24–28-month old $n = 2$, $*p < 0.05$). Magnified images of RPE flatmounts **E** 8–12-month old (Scale bar: 20 μ m), **F** 17–21-month old, and **G** 24–28-month-old *apoB100* mice showing RPE morphology and immune cell morphology. F4/80 stained images of retinal cross-sections from **H, I** 8–12-month old (Scale bar: 10 μ m) and **J, K** 17–21-month-old *apoB100* mice displaying sub-retinal immune cells (asterisks). (OPL Outer plexiform layer, ONL Outer nuclear layer, OS photoreceptor outer segments, RPE Retinal pigment epithelium).

and OCT imaging, and a severe decline in the function of RPE cells and secondary retinal neurons, the severity of which worsens with advanced age. At the ultrastructural level, the RPE cell undergoes age-dependent dysmorphic cell shape changes and phenotypic changes including loss of basal infoldings and the accumulation of intracellular lipid droplets. With the RPE morphologic changes, BrM also thickens and accumulates lipid droplets. Additionally sub-retinal immune cells accumulate in close contact with the RPE layer, with aging. This phenotype becomes more severe with age and is characterized by loss of RPE cell borders and macrophage invasion into the RPE layer itself. These mice also display an upregulation of inflammatory cytokines in the plasma and RPE-choroid, reflecting a systemic and local pro-inflammatory phenotype in the 17–21-month-old mice compared to the 8–12-month-old cohort. Since full length apoB containing lipoproteins have been identified in human BrM, drusen, and sub-RPE deposits of AMD patients, this mouse model provides a platform to investigate the role of *apoB100* in regulating a number of early

AMD-associated pathological changes, including a decline in retinal function, genesis of sub-RPE deposit formation, RPE dysmorphia, BrM changes, and local and systemic inflammation, all in the context of the risk factor of advanced age.

Our findings extend those reported by Fujihara et al. which described the morphological phenotype of *apoB100* mice for the first time³². Beyond morphology, herein we identified functional and mechanistically relevant endpoints important for the use of these mice in pre-clinical studies, including in vivo fundus and OCT imaging, retinal function, and analyses of sub-retinal and systemic inflammation at 8–12 months (middle age), 17–21 months (old age) and 24–28 months (old age). Our results highlight the contribution of age to ocular pathology. With regards to retinal function, we offer three possible theories to explain the age-associated decline observed in *apoB100* mice. First, the altered morphology of RPE cells and decreased c-wave amplitudes, which reflected RPE dysfunction, may be directly affecting the function of the overlying neurons, critical given RPE's

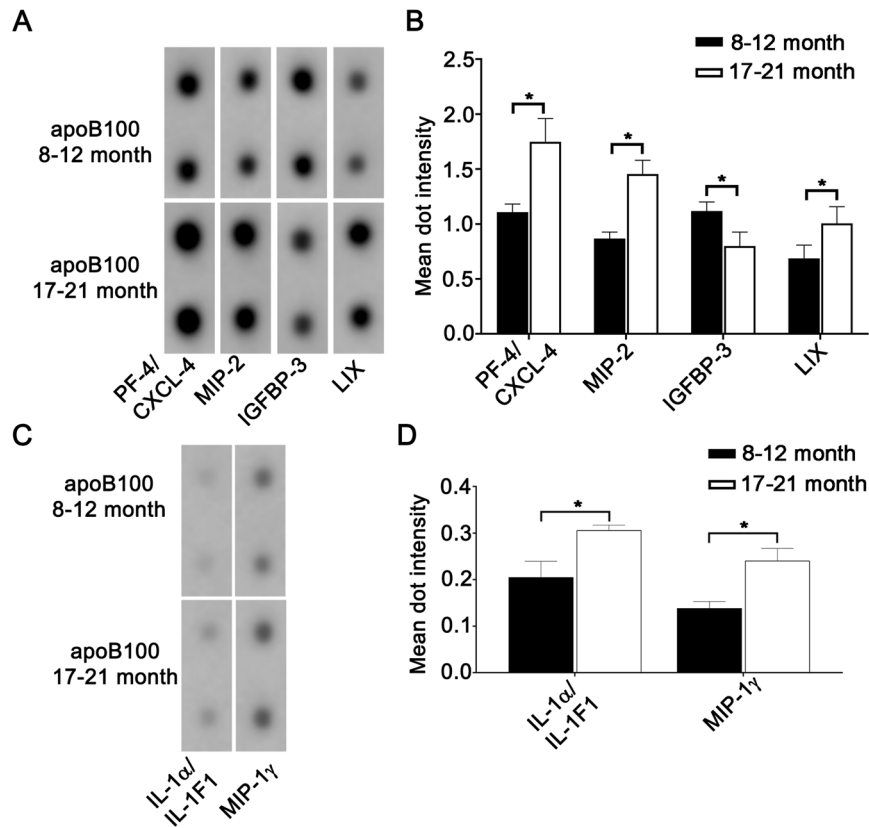


Fig. 6 Aged *apoB100* mice exhibit a significant upregulation of pro-inflammatory cytokines in the systemic circulation. Protein isolated from plasma and RPE-choroid tissue of 8–12-month and 17–21-month-old mice were blotted on a Mouse Cytokine Array C3 (62 proteins). Representative images of significantly regulated cytokines are shown. **A, B** Plasma and **(C, D)** RPE-choroid. Quantification of staining intensity of significantly regulated cytokines. ($n = 4$ per group, Mean + SEM, * $p < 0.05$, Multiple t tests).

role as nurse cells to the neurosensory retina. Second, RPE cell function loss in older mice may result from excessive lipid deposition, seen in the form of apoE-rich sub-RPE deposits and lipid droplets, contributing to an inflammatory microenvironment in the outer retina, evident by the rise of immune cells in the vicinity of RPE cell layer, sometimes, even with in the same cell layer. Finally, lipids are readily found in the retina, specifically in the rod outer segments and a dysregulation of lipid metabolism and/or clearance may be implicated in the loss of visual function as observed in the *apoB100* mice. On a systemic level, hyperlipidemia has been shown to be associated with lipaemia retinalis and reduced ERG, which was resolved when hyperlipidemia was corrected⁴⁵. Hyperlipidemia may also increase blood viscosity, cause atherosclerotic changes in retinal vessels, leading to retinal ischemia, and long term hyperlipidemia may trigger retinal morphologic changes and drop in ERG amplitudes as seen in apoE-deficient mice^{46,47}. *ApoB100* mice have been reported to present with higher levels of cholesterol in their LDL fraction, and triacylglycerol in their VLDL and LDL fractions, compared to wild-type littermates at 12–15 months of age³¹. We postulate that aging in these transgenic mice is associated with progressive accumulation of lipids in the systemic circulation making the eyes of 17–21-month-old-mice more susceptible to the detrimental effects of hyperlipidemia as compared to middle age 8–12-month-old mice.

Fujihara et al. reported that apoB100 is produced by RPE cells in these mice, a disease relevant observation as the presence of apoB100 containing lipoproteins, not apoB48, has been demonstrated in human BrM, drusen and sub-RPE deposits^{18,32}. Similarly, in our present study, ultrastructural and histological examination of the retina/RPE/choroid complex in *apoB100* mice was used to identify lipid droplets in the RPE and BrM, sub-RPE deposits and

apoE immunoreactive regions throughout BrM, a phenotype that notably worsened with age. We believe that this lipid accumulation may in part be due to progressive RPE cell dysfunction with age, leading to a decline in clearance of lipids to the choriocapillaris. With age-related BrM thickening, lipid transport is impeded and results in lipid accumulation. After synthesis by the liver, apoB100 circulates throughout the body as a component of VLDL and LDL. Similarly, the RPE cells are capable of synthesizing and secreting unique lipoprotein particles on the internal side of Bruch's membrane^{22,27,48}. The accumulation of apoE in the *apoB100* mice as a function of age, support local production of VLDL-like deposition. However, systemically derived lipoproteins may also contribute to the pathology seen in the mouse model. Mechanistically, apoB100 can bind to the LDL receptor (LDLR), leading to the internalization of cholesteryl esters from LDL into peripheral cells. The molecular players in this pathway involve LDLR and the scavenger receptor CD36, which bind to apoB protein and oxidized phospholipids, respectively, in the LDL particle^{49–51}. Alternatively, the presence of CD36 expressing-macrophage cells in close proximity to RPE cells might also be an aggravating factor in RPE dysfunction. CD36, which binds oxidized lipids, is co-expressed with the Toll-Like Receptor (TLR) 2/6 heterodimer assembly, and can sustain the TLR2/6 inflammatory signaling caused by diacylglycerols and steer TLR3-dependent macrophage driven inflammation^{52–55}. Future studies examining retinal function and ocular morphology of conditional knockout of apoB in the liver versus RPE of mice would be highly informative in delineating the contributions of local versus systemic apoB.

Inflammation is a critical mediator of AMD progression⁵⁶. In our *apoB100* mice, local and systemic inflammation appear to play a

role, as indicated by assessments of the circulating cytokine profiles and visualization of F4/80-positive macrophages concentrated in the sub-retinal space, which worsened with age. Noteworthy, the concentration of immune cells in the older *apoB100* cohort occurred in regions of RPE degeneration and atrophy. Another striking feature observed in the 17–21-month and 24–28-month-old mice was the incorporation of macrophages specifically within the RPE layer. The presence of macrophages in the outer retina has been observed in multiple models of AMD and human tissue samples^{35,57–61}, and may be a consequence of native and oxidized lipid accumulation in the outer retina sending pro-inflammatory signals, leading to recruitment of immune cells in the sub-retinal zone and the RPE layer. This scenario can potentially create a vicious cycle that aggravates inflammation, contributing to RPE degenerative changes and dysfunction, as suggested by the older *apoB100* mouse cohorts with RPE atrophy and a decline in c-wave amplitudes. *ApoB100* mice also displayed upregulated systemic levels of pro-inflammatory cytokines, including CXCL-4, MIP-2 and LIX, each with reported pro-inflammatory roles potentially contributing to the ocular pathology observed in our mouse model^{62–65}. For example, CXCL-4 has been shown to antagonize retinal neovascularization in a mouse model of oxygen-induced retinopathy (OIR)⁶⁶, is upregulated in RPE cells in response to inflammatory insults, and treatment of RPE cells with the CXCL-4 ligand, stromal cell derived factor-1 α (SDF-1 α), stimulates an increase in migration and secretion of pro-inflammatory cytokines including monocyte chemoattractant protein-1 (MCP-1), IL-8, and growth-related oncogene α ⁶⁷. At the local level the combination of age and *apoB100* expression affected the levels of two cytokines, IL-1 α , (also known as IL-1F1) and MIP-1 γ (also known as chemokine ligand 9, CCL9). Functionally, IL-1 α is a cytokine produced by monocytes and macrophages as a pro-molecule, which undergoes proteolytic processing and released in response to cell injury, as an inflammatory response⁶⁸. CCL9, a chemokine involved in the regulation of osteoclast function, has been shown to be upregulated in the RPE-choroid of aged liver-X-receptor alpha knockout mice, which show a similar abundance of immune cells in the sub-retinal space^{35,68}.

The naturally occurring mutation called retinal degeneration 8 (*rd8*), which carries a homozygous single base deletion in the crumbs homolog 1 (*Crb1*) gene, leading to formation of a truncated *Crb1* protein due to a frameshift, has been reported to be a potential confounding factor in the characterization of various mouse models of retinal degenerations³⁹. This mutation causes early onset retinal degeneration (as early as 3 months of age), retinal folds, pseudorosettes and ocular spots³⁴, which develop due to abnormalities in the adherens junctions between the photoreceptors and Müller glia cells, concentrated in the nasal quadrant. Phenotypic variations are commonly observed between and within mouse strains homozygous for the *rd8* mutation, as seen in patients carrying the *CRB1* mutation³⁹. Genotyping of our *apoB100* mouse colony revealed the presence of the *rd8* mutation. However, in contrast to the reported phenotypic features observed in the original *rd8* strain, our colony of *apoB100* mice failed to exhibit abnormal ocular morphology associated specifically with the *rd8* mutation, up to 21 months of age, the longest time point characterized in our study, using OCT images and toluidine blue staining of the retina/RPE/choroid. Pseudorosettes and retinal folds were absent in our cohort of *apoB100* mice even at 21 months of age. In contrast, the damage to the ocular pathology in the *apoB100* mice was mainly observed in the outer retina, especially at the level of RPE and did not affect the integrity of the inner retinal layers in the age groups that were analyzed. This is consistent with the observations reported in Sahu et al. which also showed that the *rd8* mutation in their study did not interfere with the phenotypic characteristics of the late-onset retinal degeneration model, generated by knocking in a heterozygous mutation in complement-1q tumor necrosis

factor-related protein 5 (*Ctrp5*) gene^{69,70}. Ultimately, that the observed pathology in the *apoB100* mice is less severe than that of mice expressing *rd8* (*Crb1*) only, raises several interesting questions regarding the interplay between *apoB100* and *rd8*, relative impact of *rd8* versus *apoB100* within the eye, and the overall vulnerability of the posterior pole, at the level of the RPE/choroid, to *rd8* versus *apoB100/rd8*, all of which would need to be investigated in detail. It is important to note, that though elevated levels of apoB100 are often referred to as the 'bad cholesterol', its primary function is still not fully understood and it is an organizing protein component of a number of other lipoproteins beyond LDL, including VLDL, Lp(a), IDL, as well as chylomicrons. In fact, recently apoB100 was found to be elevated in the aqueous of patients who required less frequent anti-VEGF injections for treatment of neovascular AMD, and choroidal neovascularization induced by laser was shown to be mitigated in *apoB100* mice relative to *B6.129* control mice supporting potential protection against neovascular AMD⁷¹.

In conclusion, we report measurable morphological and functional endpoints in a mouse model, which displays several salient features observed in AMD, exacerbated by age. Previously, young–middle age *apoB100* mice were used to test the impact of targeting the liver-X-receptor pathway on inflammation, extracellular lipid accumulation, and overall RPE health³⁵, supporting their use as a potential pre-clinical model. Given, the utility of mouse models is dependent on well defined endpoints, this model may be used as a platform for testing other etiologic factors such as cigarette smoking or high fat diet, that when combined with aging, can induce later stage phenotypic features. Likewise, this model will be valuable for testing potential therapies aimed at improving retinal function, sub-RPE deposit genesis, BrM thickening, RPE atrophy, and sub-retinal inflammation and in which advanced age plays a role.

REFERENCES

- Friedman, D. S., O'Colmain, B. J., Munoz, B., Tomany, S. C., McCarty, C., de Jong, P. T. et al. Prevalence of age-related macular degeneration in the United States. *Arch Ophthalmol* **122**, 564–572 (2004).
- Ambati, J. & Fowler, B. J. Mechanisms of age-related macular degeneration. *Neuron* **75**, 26–39 (2012).
- Li, J. Q., Welchowski, T., Schmid, M., Mauschwitz, M. M., Holz, F. G. & Finger, R. P. Prevalence and incidence of age-related macular degeneration in Europe: a systematic review and meta-analysis. *Br J Ophthalmol* **104**, 1077–1084 (2020).
- Klein, R., Peto, T., Bird, A. & Vannewkirk, M. R. The epidemiology of age-related macular degeneration. *Am J Ophthalmol* **137**, 486–495 (2004).
- DeAngelis, M. M., Owen, L. A., Morrison, M. A., Morgan, D. J., Li, M., Shikoor, A. et al. Genetics of age-related macular degeneration (AMD). *Hum Mol Genet* **26**, R246 (2017).
- Jonas, J. B., Cheung, C. M. G. & Panda-Jonas, S. Updates on the Epidemiology of Age-Related Macular Degeneration. *Asia Pac J Ophthalmol (Phila)* **6**, 493–497 (2017).
- Grassmann, F., Fauser, S. & Weber, B. H. The genetics of age-related macular degeneration (AMD)-Novel targets for designing treatment options? *Eur J Pharm Biopharm* **95**, 194–202 (2015).
- Malek, G., Yao, P.-L. & Choudhary, M. Models of Pathologies Associated with Age-Related Macular Degeneration and Their Utilities in Drug Discovery. In: Christopher L. Cioffi (ed), *Drug Delivery Challenges and Novel Therapeutic Approaches for Retinal Diseases* 10.1007/7355_2020_93 83–123 (Springer International Publishing: Cham, 2020).
- Elizabeth Rakoczy, P., Yu, M. J., Nusinowitz, S., Chang, B. & Heckenlively, J. R. Mouse models of age-related macular degeneration. *Exp Eye Res* **82**, 741–752 (2006).
- Sorsby, A. Experimental Pigmentary Degeneration of the Retina by Sodium Iodate. *Br J Ophthalmol* **25**, 58–62 (1941).
- Kannan, R. & Hinton, D. R. Sodium iodate induced retinal degeneration: new insights from an old model. *Neural Regen Res* **9**, 2044–2045 (2014).
- Moriguchi, M., Nakamura, S., Inoue, Y., Nishinaka, A., Nakamura, M., Shimazawa, M. et al. Irreversible Photoreceptors and RPE Cells Damage by Intravenous Sodium Iodate in Mice Is Related to Macrophage Accumulation. *Invest Ophthalmol Vis Sci* **59**, 3476–3487 (2018).
- Reisenhofer, M. H., Balmer, J. M. & Enzmann, V. What Can Pharmacological Models of Retinal Degeneration Tell Us? *Curr Mol Med* **17**, 100–107 (2017).

14. Malek, G., Busik, J., Grant, M. B. & Choudhary, M. Models of retinal diseases and their applicability in drug discovery. *Expert Opin Drug Discov* **13**, 359-377 (2018).
15. Hadziahmetovic, M. & Malek, G. Age-Related Macular Degeneration Revisited: From Pathology and Cellular Stress to Potential Therapies. *Front Cell Dev Biol* **8**, 612812 (2020).
16. Choudhary, M. & Malek, G. A Review of Pathogenic Drivers of Age-Related Macular Degeneration, Beyond Complement, with a Focus on Potential Endpoints for Testing Therapeutic Interventions in Preclinical Studies. *Adv Exp Med Biol* **1185**, 9-13 (2019).
17. Choudhary, M. & Malek, G. Rethinking Nuclear Receptors as Potential Therapeutic Targets for Retinal Diseases. *J Biomol Screen* **21**, 1007-1018 (2016).
18. Curcio, C. A., Johnson, M., Huang, J. D. & Rudolf, M. Apolipoprotein B-containing lipoproteins in retinal aging and age-related macular degeneration. *J Lipid Res* **51**, 451-467 (2010).
19. Wang, L., Clark, M. E., Crossman, D. K., Kojima, K., Messinger, J. D., Mobley, J. A. et al. Abundant lipid and protein components of drusen. *PLoS One* **5**, e10329 (2010).
20. Rudolf, M. & Curcio, C. A. Esterified cholesterol is highly localized to Bruch's membrane, as revealed by lipid histochemistry in whole mounts of human choroid. *J Histochem Cytochem* **57**, 731-739 (2009).
21. Curcio, C. A., Millican, C. L., Bailey, T. & Kruth, H. S. Accumulation of cholesterol with age in human Bruch's membrane. *Invest Ophthalmol Vis Sci* **42**, 265-274 (2001).
22. Curcio, C. A., Johnson, M., Rudolf, M. & Huang, J. D. The oil spill in ageing Bruch membrane. *Br J Ophthalmol* **95**, 1638-1645 (2011).
23. Klaver, C. C., Kliffen, M., van Duijn, C. M., Hofman, A., Cruts, M., Grobbee, D. E. et al. Genetic association of apolipoprotein E with age-related macular degeneration. *Am J Hum Genet* **63**, 200-206 (1998).
24. Ebrahimi, K. B. & Handa, J. T. Lipids, lipoproteins, and age-related macular degeneration. *J Lipids* **2011**, 802059 (2011).
25. Malek, G., Li, C. M., Guidry, C., Medeiros, N. E. & Curcio, C. A. Apolipoprotein B in cholesterol-containing drusen and basal deposits of human eyes with age-related maculopathy. *Am J Pathol* **162**, 413-425 (2003).
26. Li, C. M., Clark, M. E., Chimento, M. F. & Curcio, C. A. Apolipoprotein localization in isolated drusen and retinal apolipoprotein gene expression. *Invest Ophthalmol Vis Sci* **47**, 3119-3128 (2006).
27. Pikuleva, I. A. & Curcio, C. A. Cholesterol in the retina: the best is yet to come. *Prog Retin Eye Res* **41**, 64-89 (2014).
28. Holz, F. G., Sheraidah, G., Pauelikhoff, D. & Bird, A. C. Analysis of lipid deposits extracted from human macular and peripheral Bruch's membrane. *Arch Ophthalmol* **112**, 402-406 (1994).
29. Ruberti, J. W., Curcio, C. A., Millican, C. L., Menco, B. P., Huang, J. D. & Johnson, M. Quick-freeze/deep-etch visualization of age-related lipid accumulation in Bruch's membrane. *Invest Ophthalmol Vis Sci* **44**, 1753-1759 (2003).
30. Volland, S., Esteve-Rudd, J., Hoo, J., Yee, C. & Williams, D. S. A comparison of some organizational characteristics of the mouse central retina and the human macula. *PLoS One* **10**, e0125631 (2015).
31. Farese, R. V., Jr., Veniant, M. M., Cham, C. M., Flynn, L. M., Pierotti, V., Loring, J. F. et al. Phenotypic analysis of mice expressing exclusively apolipoprotein B48 or apolipoprotein B100. *Proc Natl Acad Sci U S A* **93**, 6393-6398 (1996).
32. Fujihara, M., Cano, M. & Handa, J. T. Mice that produce ApoB100 lipoproteins in the RPE do not develop drusen yet are still a valuable experimental system. *Invest Ophthalmol Vis Sci* **55**, 7285-7295 (2014).
33. Hu, P., Herrmann, R., Bednar, A., Saloupis, P., Dwyer, M. A., Yang, P. et al. Aryl hydrocarbon receptor deficiency causes dysregulated cellular matrix metabolism and age-related macular degeneration-like pathology. *Proc Natl Acad Sci U S A* **110**, E4069-4078 (2013).
34. Mehalow, A. K., Kameya, S., Smith, R. S., Hawes, N. L., Denegre, J. M., Young, J. A. et al. CRB1 is essential for external limiting membrane integrity and photoreceptor morphogenesis in the mammalian retina. *Hum Mol Genet* **12**, 2179-2189 (2003).
35. Choudhary, M., Ismail, E. N., Yao, P. L., Tayyari, F., Radu, R. A., Nusinowitz, S. et al. LXRs regulate features of age-related macular degeneration and may be a potential therapeutic target. *JCI Insight* **5** (2020).
36. Prusky, G. T., Alam, N. M., Beekman, S. & Douglas, R. M. Rapid quantification of adult and developing mouse spatial vision using a virtual optomotor system. *Invest Ophthalmol Vis Sci* **45**, 4611-4616 (2004).
37. Claybon, A. & Bishop, A. J. Dissection of a mouse eye for a whole mount of the retinal pigment epithelium. *J Vis Exp* <https://doi.org/10.3791/2563> (2011).
38. Choudhary, M., Safe, S. & Malek, G. Suppression of aberrant choroidal neovascularization through activation of the aryl hydrocarbon receptor. *Biochim Biophys Acta Mol Basis Dis* **1864**, 1583-1595 (2018).
39. Mattapallil, M. J., Wawrousek, E. F., Chan, C. C., Zhao, H., Roychoudhury, J., Ferguson, T. A. et al. The Rd8 mutation of the Crb1 gene is present in vendor lines of C57BL/6N mice and embryonic stem cells, and confounds ocular induced mutant phenotypes. *Invest Ophthalmol Vis Sci* **53**, 2921-2927 (2012).
40. Yonehara, K., Shintani, T., Suzuki, R., Sakuta, H., Takeuchi, Y., Nakamura-Yonehara, K. et al. Expression of SPIG1 reveals development of a retinal ganglion cell subtype projecting to the medial terminal nucleus in the mouse. *PLoS One* **3**, e1533 (2008).
41. Kretschmer, F., Tariq, M., Chatila, W., Wu, B. & Badea, T. C. Comparison of optomotor and optokinetic reflexes in mice. *J Neurophysiol* **118**, 300-316 (2017).
42. Oyster, C. W., Takahashi, E. & Collewijn, H. Direction-selective retinal ganglion cells and control of optokinetic nystagmus in the rabbit. *Vision Res* **12**, 183-193 (1972).
43. Curcio, C. A., Johnson, M., Huang, J. D. & Rudolf, M. Aging, age-related macular degeneration, and the response-to-retention of apolipoprotein B-containing lipoproteins. *Prog Retin Eye Res* **28**, 393-422 (2009).
44. Anderson, D. H., Ozaki, S., Nealon, M., Neitz, J., Mullins, R. F., Hageman, G. S. et al. Local cellular sources of apolipoprotein E in the human retina and retinal pigmented epithelium: implications for the process of drusen formation. *Am J Ophthalmol* **131**, 767-781 (2001).
45. Lu, C. K., Chen, S. J., Niu, D. M., Tsai, C. C., Lee, F. L. & Hsu, W. M. Electrophysiological changes in lipaemia retinalis. *Am J Ophthalmol* **139**, 1142-1145 (2005).
46. Ong, J. M., Zorapapel, N. C., Aoki, A. M., Brown, D. J., Nesburn, A. B., Rich, K. A. et al. Impaired electroretinogram (ERG) response in apolipoprotein E-deficient mice. *Curr Eye Res* **27**, 15-24 (2003).
47. Plump, A. S., Smith, J. D., Hayek, T., Aalto-Setälä, K., Walsh, A., Verstuyft, J. G. et al. Severe hypercholesterolemia and atherosclerosis in apolipoprotein E-deficient mice created by homologous recombination in ES cells. *Cell* **71**, 343-353 (1992).
48. Curcio, C. A. Soft Drusen in Age-Related Macular Degeneration: Biology and Targeting Via the Oil Spill Strategies. *Invest Ophthalmol Vis Sci* **59**, AMD160-AMD181 (2018).
49. Hayes, K. C., Lindsey, S., Stephan, Z. F. & Brecker, D. Retinal pigment epithelium possesses both LDL and scavenger receptor activity. *Invest Ophthalmol Vis Sci* **30**, 225-232 (1989).
50. Ryeom, S. W., Silverstein, R. L., Scotto, A. & Sparrow, J. R. Binding of anionic phospholipids to retinal pigment epithelium may be mediated by the scavenger receptor CD36. *J Biol Chem* **271**, 20536-20539 (1996).
51. Ryeom, S. W., Sparrow, J. R. & Silverstein, R. L. CD36 participates in the phagocytosis of rod outer segments by retinal pigment epithelium. *J Cell Sci* **109** (Pt 2), 387-395 (1996).
52. Reis, A., Mateus, C., Melo, P., Figueira, J., Cunha-Vaz, J. & Castelo-Branco, M. Neuroretinal dysfunction with intact blood-retinal barrier and absent vasculopathy in type 1 diabetes. *Diabetes* **63**, 3926-3937 (2014).
53. Feng, L., Ju, M., Lee, K. Y. V., Mackey, A., Evangelista, M., Iwata, D. et al. A Proinflammatory Function of Toll-Like Receptor 2 in the Retinal Pigment Epithelium as a Novel Target for Reducing Choroidal Neovascularization in Age-Related Macular Degeneration. *Am J Pathol* **187**, 2208-2221 (2017).
54. Beutler, B., Jiang, Z., Georgel, P., Crozat, K., Croker, B., Rutschmann, S. et al. Genetic analysis of host resistance: Toll-like receptor signaling and immunity at large. *Annu Rev Immunol* **24**, 353-389 (2006).
55. Huh, H. Y., Pearce, S. F., Yesner, L. M., Schindler, J. L. & Silverstein, R. L. Regulated expression of CD36 during monocyte-to-macrophage differentiation: potential role of CD36 in foam cell formation. *Blood* **87**, 2020-2028 (1996).
56. Miller, J. W., Bagheri, S. & Vavvas, D. G. Advances in Age-related Macular Degeneration Understanding and Therapy. *US Ophthalmic Rev* **10**, 119-130 (2017).
57. Hollyfield, J. G., Bonilha, V. L., Rayborn, M. E., Yang, X., Shadrach, K. G., Lu, L. et al. Oxidative damage-induced inflammation initiates age-related macular degeneration. *Nat Med* **14**, 194-198 (2008).
58. Cruz-Guilloty, F., Saeed, A. M., Echegaray, J. J., Duffort, S., Ballmick, A., Tan, Y. et al. Infiltration of proinflammatory m1 macrophages into the outer retina precedes damage in a mouse model of age-related macular degeneration. *Int J Inflamm* **2013**, 503725 (2013).
59. Ban, N., Lee, T. J., Sene, A., Choudhary, M., Lekwuwa, M., Dong, Z. et al. Impaired monocyte cholesterol clearance initiates age-related retinal degeneration and vision loss. *JCI Insight* **3** (2018).
60. Sennlaub, F., Auvynet, C., Calippe, B., Lavalette, S., Poupel, L., Hu, S. J. et al. CCR2 (+) monocytes infiltrate atrophic lesions in age-related macular disease and mediate photoreceptor degeneration in experimental subretinal inflammation in Cx3cr1 deficient mice. *EMBO Mol Med* **5**, 1775-1793 (2013).
61. Combadiere, C., Feumi, C., Raoul, W., Keller, N., Rodero, M., Pezard, A. et al. CX3CR1-dependent subretinal microglia cell accumulation is associated with cardinal features of age-related macular degeneration. *J Clin Invest* **117**, 2920-2928 (2007).
62. Kobayashi, Y. The role of chemokines in neutrophil biology. *Front Biosci* **13**, 2400-2407 (2008).

63. Kaplan, R. C., McGinn, A. P., Pollak, M. N., Kuller, L. H., Strickler, H. D., Rohan, T. E. *et al.* Association of total insulin-like growth factor-I, insulin-like growth factor binding protein-1 (IGFBP-1), and IGFBP-3 levels with incident coronary events and ischemic stroke. *J Clin Endocrinol Metab* **92**, 1319-1325 (2007).
64. Gomez, J. M., Maravall, F. J., Gomez, N., Navarro, M. A., Casamitjana, R. & Soler, J. The IGF-I system component concentrations that decrease with ageing are lower in obesity in relationship to body mass index and body fat. *Growth Horm IGF Res* **14**, 91-96 (2004).
65. Kielczewski, J. L., Hu, P., Shaw, L. C., Li Calzi, S., Mames, R. N., Gardiner, T. A. *et al.* Novel protective properties of IGFBP-3 result in enhanced pericyte ensheathment, reduced microglial activation, increased microglial apoptosis, and neuronal protection after ischemic retinal injury. *Am J Pathol* **178**, 1517-1528 (2011).
66. Cai, S., Yang, Q., Cao, Y., Li, Y., Liu, J., Wang, J. *et al.* PF4 antagonizes retinal neovascularization via inhibiting PRAS40 phosphorylation in a mouse model of oxygen-induced retinopathy. *Biochim Biophys Acta Mol Basis Dis* **1866**, 165604 (2020).
67. Crane, I. J., Wallace, C. A., McKillop-Smith, S. & Forrester, J. V. CXCR4 receptor expression on human retinal pigment epithelial cells from the blood-retina barrier leads to chemokine secretion and migration in response to stromal cell-derived factor 1 alpha. *J Immunol* **165**, 4372-4378 (2000).
68. Wooff, Y., Man, S. M., Aggio-Bruce, R., Natoli, R. & Fernando, N. IL-1 Family Members Mediate Cell Death, Inflammation and Angiogenesis in Retinal Degenerative Diseases. *Front Immunol* **10**, 1618 (2019).
69. Sahu, B., Chavali, V. R., Alapati, A., Suk, J., Bartsch, D. U., Jablonski, M. M. *et al.* Presence of rd8 mutation does not alter the ocular phenotype of late-onset retinal degeneration mouse model. *Mol Vis* **21**, 273-284 (2015).
70. Chavali, V. R., Khan, N. W., Cukras, C. A., Bartsch, D. U., Jablonski, M. M. & Ayyagari, R. A CTRP5 gene S163R mutation knock-in mouse model for late-onset retinal degeneration. *Hum Mol Genet* **20**, 2000-2014 (2011).
71. Cao, X., Sanchez, J. C., Dinabandhu, A., Guo, C., Patel, T. P., Yang, Z. *et al.* Aqueous proteins help predict the response of patients with neovascular age-related macular degeneration to anti-VEGF therapy. *J Clin Invest* **132** (2022).

ACKNOWLEDGEMENTS

J.T.H. is the Robert Bond Welch Professor. We thank Dr. Neal Peachy for assistance with the c-wave recording protocols and Mr. Michael Lekwuwa for technical support.

AUTHOR CONTRIBUTIONS

M.C., J.T.H., and G.M. contributed to the conception and design of the study, data interpretation, and paper editing. M.C., F.T., and J.T.H. conducted experiments, collected, and analyzed data. M.C. and G.M. contributed to paper writing. All authors approved the final version of the submitted paper.

FUNDING

This research was supported by funding from the National Eye Institute: EY027802 (G. M.), EY028160 (G.M.), EY032751 (G.M.), EY027691 (J.T.H.), P30 EY005722 (Duke Eye Center), a Research to Prevent Blindness, Inc (RPB) Core grant (Duke Eye Center), and an unrestricted RPB grant (Wilmer Eye Institute).

COMPETING INTERESTS

J.T.H. received grant funding and royalties from Bayer Pharmaceuticals, Inc, and grant funding and stock options as a member of the Scientific Advisory Board for Clover Pharmaceuticals, Inc, both for unrelated projects.

ETHICS APPROVAL

Study protocols were approved by the Duke University and Johns Hopkins Institutional Animal Care and Use Committees. All animal experiments were performed in accordance with the guidelines of the Association for Research in Vision and Ophthalmology (ARVO) statement for the Use of Animals in Ophthalmic and Vision Research.

ADDITIONAL INFORMATION

Supplementary information The online version contains supplementary material available at <https://doi.org/10.1038/s41374-022-00795-7>.

Correspondence and requests for materials should be addressed to Goldis Malek.

Reprints and permission information is available at <http://www.nature.com/reprints>

Publisher's note Springer Nature remains neutral with regard to jurisdictional claims in published maps and institutional affiliations.